Spatial Optical Modulator (SOM) : Samsung's Light Modulator for the Next Generation Laser Display

Sang Kyeong Yun*, JongHyeong Song, Tae-won Lee, Injae Yeo, Yoonjoon Choi, Yeonggyu Lee, Seungdo An, Kyubum Han, Yurlov Victor, Heung-Woo Park, Changsu Park, Heeyeoun Kim, JeongSuong Yang, Jongpil Cheong, Seungwon Ryu, Kwanyoung Oh, Haengseok Yang, Yoonshik Hong, Seokkee Hong, Sangkee Yoon, Jaewook Jang, Jehong Kyoung, Ohkkun Lim, Chungi Kim, Anatoliy Lapchuk, Shyshkin Ihar, Seungwoo Lee, Sunki Kim, Youngnam Hwang, Kisuk Woo, Seungwan Shin, Jungchul Kang, Dong-Hyun Park

SOM Team, Central R&D Institute, Samsung Electro-Mechanics Co,
314 Meatan3-Dong, Yeongtong-Gu, Suwon, Gyunggi-Do, R.O. Korea 443-743
*** Phone: 82-31-210-5861, E-mail: nano.yun@samsung.com**

Abstract

A new type of diffractive spatial optical modulators, named SOM, has been developed by Samsung Electro-Mechanics for projection display and other applications. A laser display in full HD format (1920x1080) was successfully demonstrated by using prototype projection engines having SOM devices, signal processing circuits, and projection optics.

1. Objectives and Background

Spatial light modulators (SLM) are of growing interests due to the great success of Texas Instruments' (TI) Digital Micro-Mirror Device (DMD) in high-resolution projection displays [1]. Owing to their variety of applications, several SLMs are developed including the Grating Light Valve (GLV) [2] and Grating Electromechanical System (GEMS) [3] with faster response and higher light modulation performance.

This paper describes the structure, operation, performance, and laser-display applications of a diffractive SLM, named "Spatial Optical Modulator (SOM)", currently under development by the Samsung Electro-Mechanics.

2, General operation principles

Optical modulation scheme and detailed ribbon structure of the SOM are shown in Fig 1.

The individual pixel of the SOM can be optically modeled as a dynamic reflection phase grating.

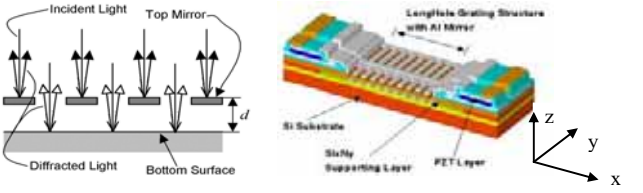

Fig 1. The optical modulation scheme and the single –pixel ribbon structure of SOM

When a monochromatic beam is incident on the SOM, it is diffracted into multiple spatial-harmonic orders. By controlling the position of the upper mirror with respect to the bottom reflector, the diffracted energy can be re-distributed between 0^{th} and 1^{st} diffraction orders.

As shown in Fig. 1, SOM utilizes the piezoelectric actuation of individual grating micro-mirror to control the displacement between the upper micro-mirror and the bottom reflector to achieve the variable phase shift, providing the diffractive light modulation. A mechanical actuation displacement within one quarter of a wavelength is sufficient to fully modulate the diffracted light with high contrast.

The advantages of using piezoelectric transducers for MEMS devices include low energy loss, fast response, low operating voltage, and good signal-to-noise ratio, in comparison with other operation principles such as the electrostatic, electromagnetic, and thermal conversion. The actuator consists of a thin structural material supporting a PZT film sandwiched between top and bottom electrodes.

A simplified optical schematic diagram of the display single color channel is described in Fig. 2. Light source can be Optically Pumped Semiconductor Laser (OPSL) based on Vertical External Cavity Surface-Emitting Laser (VECSEL) as well as a single Laser Diode (LD) or LD array. In the case of using the LD as a pair of collimator – cylinder lenses are needed to form on the SOM linearly focused light beam which after reflection is divided into two symmetrical diffraction orders. These orders come through projection lens, Schlieren stop and reflecting from scanning mirror approach the screen where the SOM array magnified image is reconstructed. SOM array is perpendicular to the picture plane and scanning mirror rotation is in picture plane. Three color display diagram may be obtained by combining three illumination parts and three SOMs using either dichroic mirrors or X-cube.

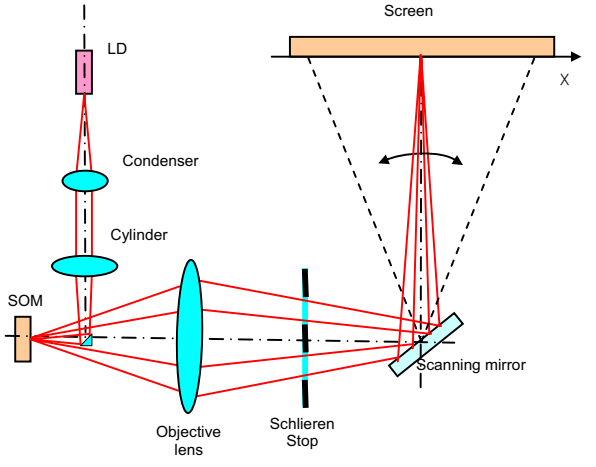

Fig. 2. The Conceptual optical schematic diagram of the SOM –based projection display (Top view, single color)

The SOM has a 2D diffraction structure. The main diffraction structure is distributed along X axis and consists of number of holes and intervals between holes. Pixel array is distributed along Y axis and consists of ribbons or beams suspended over the bottom. Diffraction maximums are deflected in two dimensions: along X and Y directions. The scheme of such complicated diffraction process is presented at Fig. 3 where the sphere of radius $k = 2\pi/\lambda$ and wave vectors corresponding to diffraction orders are presented. Each diffraction order has double index corresponding to the numbers of maxima in both directions. All diffracted vectors lay on conical surfaces even in the case of normal incidence.

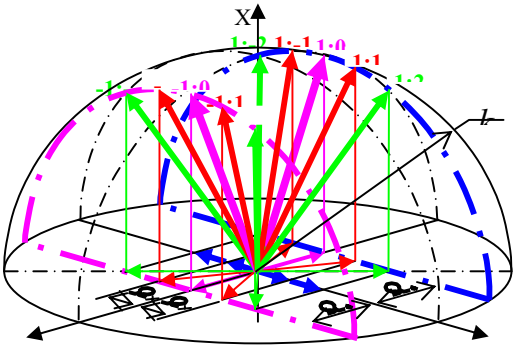

Fig 3. The scheme of diffraction on 2D

3. Diffraction process in SOM

Diffracted fields from the SOM at any distance can be expressed by a Fourier transform as

$$S(x,y,z) = \frac{1}{4\pi^2}\iint F(u,v,z)\exp\left[j(ux+vy)\right]dudv \qquad (1)$$

where $u = k\cos\alpha$ and $v = k\cos\beta$ are spatial frequencies, α and β are the angles between spatial harmonic wave vector and x and y axis, respectively, and $k = 2\pi/\lambda$ is the wave number. F(u,v,z), may be obtained using the free space transfer function (FSTF) as [4]

$$F(u,v,z) = F_r(u,v)FSTF(u,v,z) \qquad (2)$$

where

$$FSTF(u,v,z) = e^{jz(k^2-u^2+v^2)^{1/2}} \qquad (3)$$

The Fourier transform $F_r(u,v)$ is given by

$$F_r(u,v) = \iint S_r(x,y)e^{-j(ux+vy)}dxdy \qquad (4)$$

and

$$S_r(x,y) = S_{up}(x,y) + S_{dn}(x,y) \qquad (5)$$

where $S_r(x,y)$ is the complex field amplitude reflected from the SOM defined in the z = 0 plane. It includes two field components; the reflected field $S_{up}(x,y)$ from the top mirror and $S_{dn}(x,y)$ from the bottom-mirror surface.

Reflected field amplitude from the upper mirror may be expressed by Eq. (6),

$$S_{up}(x,y) = S_i(x,y)r(x,y) \qquad (6)$$

where

$S_i(x,y)$ – incident field

Ribbon reflection function r(x,y) can be given by

$$r(x,y)=\begin{cases}0 & \text{, open region in the upper mirror}\\ 1 & \text{, otherwise}\end{cases}$$

Transmitted field amplitude through upper ribbon hole beam into the inner space may be represented, both in spatial and frequency domain, respectively, as

$$S_1(x,y)=S_i(x,y)t(x,y) \qquad (7)$$

$$F_1(u,v)=\iint S_1(x,y)e^{-j(ux+vy)}dxdy \qquad (8)$$

where t(x,y) = 1 – r(x,y) is the ribbon transmittance function.

The transmitted beam is propagated to the bottom mirror, reflected from the bottom surface, and propagated back to the upper mirror surface resulting in a total propagation distance of 2h. The field amplitude experiencing the round trip may be represented, using FSTF in the frequency domain, as

$$F_2(u,v)=F_1(u,v)FSTF(u,v,2h) \qquad (9)$$

The optical field (9) once again, passes through the upper ribbon hole and after vignetting may be presented as 2D convolution in spatial frequency domain by

$$F_{dn}(u,v)=\frac{1}{4\pi^2}\iint F_2(u',v')T(u-u',v-v')du'dv' \qquad (10)$$

where T(u,v) is the Fourier transform of the transmittance function t(x,y). Inverse Fourier transformation of Eq. (10) gives us reflected optical field from the bottom reflector in spatial domain as

$$S_{dn}(x,y)=\frac{1}{4\pi^2}\iint F_{dn}(u,v)e^{j(ux+vy)}dudv \qquad (11)$$

The total reflected field from the SOM in the XY plane can be obtained by substituting Eqs. (6) and (11) into Eq. (5) and then into Eq. (4).

The diffraction pattern calculated using Eqs. (1)-(5) for the non-actuated and actuated states are shown in Fig. 4. When the SOM is in non-actuated state as Fig 4 (a), all optical power is concentrated in the zero diffraction order. When the SOM is in the actuated state as Fig 3 (b) incoming optical power is divided mostly into $+1^{st}$ and -1^{st} diffraction orders.

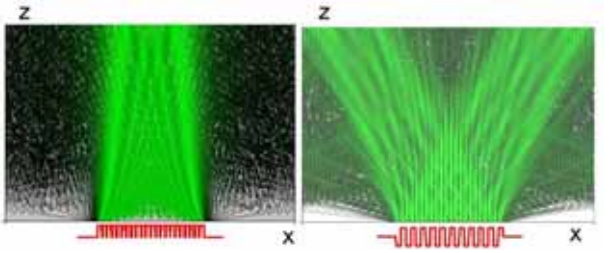

(a) (b)

Fig. 4. Calculated diffraction patterns from the SOM (a) at the non-actuated state and (b) the actuated state.

Figure 5 shows the diffraction mechanism in the SOM inner space using intensity and phase distributions separately for the incident and the reflected beams, respectively. It also shows the cross-section of single SOM pixel in XZ plane perpendicular to the grooves of the main diffraction structure.

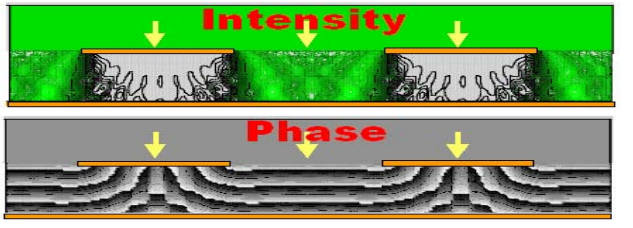

(a) Incident beam intensity (above) and phase (below) distributions

(b) Reflected beam intensity (above) and phase (below)

Fig. 5 Diffraction effects in the inner space between the top mirror and the bottom reflector and in the near field zone (Actuated state).

Intensity distributions at Fig 5 show us loss during vignetting in the holes. Phase distributions at Fig. 5 illustrate wavefronts shapes and diffraction divergence.

In detail, the amplitude and phase distribution of the total reflected field from (5), (6) and (11) are presented in Fig. 6 for two ribbon displacements corresponding to non-actuated (h=2λ) and the fully actuated state (h=2.25λ) of the SOM. In Fig 6, we can

see the difference between light beam portions reflected from the top and the bottom mirror surfaces both in amplitude and phase. This difference destructs the balance between top and bottom reflected components in all diffraction orders. The phase misbalance means that the minimum diffraction efficiency for the 1st diffraction order in the dark state occurs at a displacement value, h, different from the expected value h = $(2n)(\lambda/4)$, where n=0,1,2.. is integer number. This difference is generally very small (several nm) and can be ignored in most practical cases.

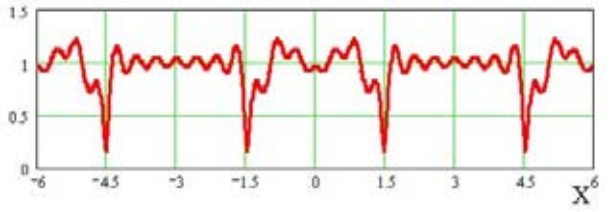

(a) Amplitude (actuated SOM)

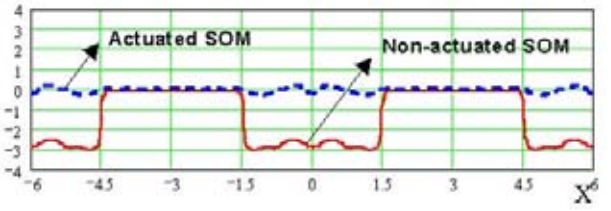

(b) Phase

Fig. 6. Reflected beam amplitude and phase distribution along the x axis.

The amplitude misbalance may cause a more serious effect. As mentioned before, the existing amplitude misbalance provides decrease of contrast ratio even for an ideally fabricated SOM device. Furthermore, increase in amplitude misbalance results in decrease of contrast ratio.

At the same time amplitude misbalance may be compensated by changing relationship between hole and ridge sizes in the upper ribbon

In practice contrast ratio depends on many factors. Such factors may be not only diffraction inside SOM, size tolerances and ribbon bending, as we noted before, but also ribbon height non-uniformity remained after SOM calibration, background due to parasitic reflections and scattering.

Table 1. Diffraction efficiency and contrast ratio calculated by scalar diffraction theory.

Fill factor (%)	Efficiency (%)[3]	C/R limit (Full Screen)[4]	Concerned diffraction order
71[1]	46	6,000	(1,1), (1,0), (1,-1)
88[2]	58	4,000	(-1,1), (-1,0), (-1,-1)

1080p SOM with its pixel pitch 21 um (1) frame width=2 um, gap between ribbon=2 um, (2) frame width=1 um, gap between ribbon=0.5 um, (3) ideal structure with mirror reflectivity of 92 %, (4) assumed background noise level: 10^{-5}

Calculated diffraction efficiency and contrast ratio using the scalar diffraction theory are summarized in Table 1. The fill factor used in the table represents the effective portion of the SOM reflective area that provides contribution into operating diffraction orders.

4. SOM fabrication

The SOM was fabricated using the well-established surface micromachining technique. Optimal structural dimensions were found through optical diffraction and mechanical FEM simulations. Typical natural frequency and maximum displacement of the fabricated SOM ribbon are ~500 kHz and ~400 nm, respectively. The ribbon displacement depending on the applied bias is shown in Fig. 7 (a). The ribbon damping can be optimized by simple control of the ribbon-gap height in Fig. 7(b). The flatness level of Al coated on SiN ribbon is important for optical performance of the SOM and can be obtained by precise control of the stress balance between two composition layers.

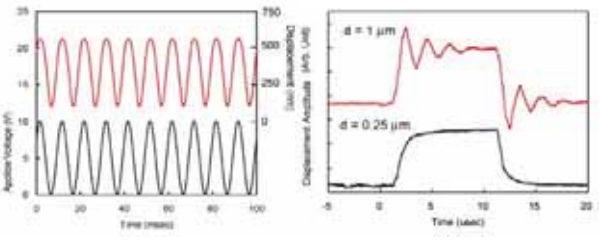

(a) (b)

Fig. 7. (a) Displacement response of the piezo-actuated SOM bridge structure. (b) The step displacement responses of the SOM ribbons with different sacrificial layer thickness.

The dedicated SOM driver ICs was exclusively developed to optimize the driving signals, which were flip-chip bonded with a 1080-pixel SOM chip. Flip-chip bonded package, shown in Fig. 8, implies smaller package size and higher reliability in interconnection compared with those of the wire-bonded package.

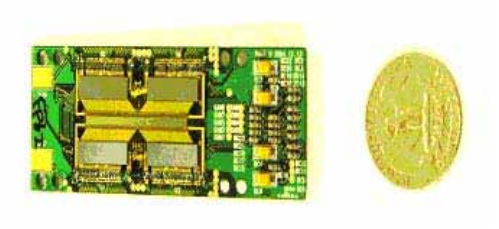

Fig. 8. Packaged 1080pixel SOM modules with a coin for comparison.

5. Summary

SOM-based laser rear projection engine prototype was developed and demonstrated. The laser primaries used were OPSL-type VECSELs for blue (457 nm, 1.0 W) and green (532 nm, 1.0 W) channels and LD array (635 nm, 1.2 W) for red channel. Each beam coming from lasers was shaped by the anamorphic (astigmatic) illumination optics to have a uniform linear shaped beam, which size was matched to the active area of the SOM panel. For blue and green channel the identical illumination systems were used while for red channel having LD array from 7 LD illumination system was different and comprised fly-eye micro-cylindrical lens array. All illumination systems have different efficiencies.

For 3 different color channels 3 identical SOMs were used, and two dichroic mirrors for different color beam combining were introduced in optical path after SOMs.

For all colors single projection and scanning system was employed. Scanning frequency was 60 frames per second. Image was projected on standard plastic screen for rear projection displays with 60 inches in diagonal size.

Fig. 9. Displayed screen image using a prototype rear projection optical engine and control circuit.

Using prototype full HD SOM laser rear projection display, we successfully demonstrated seamless images in the full HD resolution (1920 x 1080) with rich, vivid colors implementing 8-bits gray scale per color channel. Generated screen image is shown in Fig. 9

With the novel device features, the developed SOM provides a new approach to high quality laser projection display.

4. References

[1] L. A. Yoder, An Introduction to the Digital Light Processing Technology, WWW Document, (http://dlp.com/dlp_technology/dlp_technology_white_papers.asp)

[2] J. I. Trisnadi, C. B. Carlisle and R. Monteverde, MOEMS Display and Imaging Systems II (SPIE, USA, 2004).

[3] J. C. Brazas, and M. W. Kowarz, MOEMS Display and Imaging Systems II, edited by H. Urey, D. L. Dickensheets (SPIE, USA, 2004)

[4] J. W. Goodman. Introduction to Fourier Optics (2nd edition), McGraw-Hill, New York (1996)